Liquid Crystals
Publication details, including instructions for authors and subscription information:
http://www.informaworld.com/smpp/title~content=t713926090

Novel memory effect found in nematic liquid crystal/fine particle system

Masaya Kawasumi[a]; Naoki Hasegawa[a]; Arimitsu Usuki[a]; Akane Okada[a]
[a] Toyota Central Research and Development Laboratories, Inc., Aichi, Japan

To cite this Article Kawasumi, Masaya , Hasegawa, Naoki , Usuki, Arimitsu and Okada, Akane(1996) 'Novel memory effect found in nematic liquid crystal/fine particle system', Liquid Crystals, 21: 6, 769 — 776
To link to this Article: DOI: 10.1080/02678299608032892
URL: http://dx.doi.org/10.1080/02678299608032892

LIQUID CRYSTALS, 1996, VOL. 21, NO. 6, 769–776

Novel memory effect found in nematic liquid crystal/fine particle system

by MASAYA KAWASUMI*, NAOKI HASEGAWA, ARIMITSU USUKI and AKANE OKADA

Toyota Central Research and Development Laboratories, Inc., Nagakute-cho, Aichi, 480-11, Japan

(*Received 22 May 1996; accepted 15 July 1996*)

Novel liquid crystalline composites composed of a nematic two-frequency-addressing liquid crystal and organized clay mineral (about 1 wt %) have been prepared. The particles of clay mineral were dispersed homogeneously in the liquid crystal. The composite cells became transparent within 50 ms when a 60 Hz electric field was applied. The transparent state was maintained after the field was switched off. It transformed into a turbid light scattering state by applying 1·5 kHz electric field which caused dynamic scattering in the cell. The light transmittance of both memory states did not change after 20 h without the electric field.

1. Introduction

The optical memory effects of cholesteric and smectic liquid crystalline materials based on light scattering have been reported in several electro-optical systems. The existence of a memory effect in cholesterics has been evidenced by Heilmeier and Goldmacher [1]; when subjected to a d.c. or low frequency electric field, a cholesteric structure with small pitch can be switched from a transparent state to a turbid light scattering state. When the field is turned off, the scattering state is still observed for several hours. It can be switched back to the transparent state by the application of a high frequency electric field, thus exhibiting a reversible switch. A similar memory effect has been found in smectic mixtures of polymeric liquid crystals with low molar mass liquid crystals by Kajiyama *et al.* [2]. In the case of nematic liquid crystals, most systems do not exhibit such a memory effect due to their low viscosity, with the exception of a few examples. Polymer dispersed nematic liquid crystals with a polyball-type morphology have been reported to exhibit a memory effect [3]. In this case, the transparent memory state can be cancelled to a scattering state only by a thermal treatment. The other examples [4, 5] use surface effects to produce the memory effect, although they are not based on light scattering.

Recently, we have demonstrated a novel approach to add a memory effect to nematic liquid crystals by applying a hybrid technique with inorganic fine particles [6]. The novel liquid crystalline composite (LCC) based on a nematic low molar mass liquid crystals and a fine plate-like clay mineral, i.e. montmorillonite intercalated with a mesogenic ammonium ion, has displayed a unique light scattering effect as follows. Initially, the cell scattered light strongly. When an electric field was applied to the cell, it became transparent within 10–20 ms. After the electric field was switched off, although a small decrease in the transparency was observed, the transparent state was maintained over 3 months. However, in order to cancel the transparent memory state to the initial light scattering state, a slight shearing should be given to the substrates of the cell.

In this paper, we have prepared novel LCCs based on a nematic two-frequency-addressing liquid crystal (TFALC). The TFALC is a liquid crystal with regimes of positive dielectric anisotropy as well as negative dielectric anisotropy. Therefore, the molecular alignment of a TFALC can be controlled actively by changing the frequency of the electric field. This unique nature of a TFALC was used for the electrically reversible optical switching of the LCCs. The novel LCCs based on the TFALC have actually displayed a bistable and reversible light scattering electro-optic effect.

2. Experimental

2.1. *Materials*

The materials used for the preparation of LCCs are nematic TFALC (DF-05XX) from Chisso Co. and purified montmorillonite (Kunipia-F) from Kunimine Co. The physical properties of the TFALC are listed in the table. The TFALC is a mixture of low molar mass liquid crystals with regimes of positive dielectric anisotropy as

*Author for correspondence.

0267–8292/96 $12·00

Table Physical properties of two-frequency-addressing liquid crystalline mixture used in the experiments.

Parameter		DF-05XX
Nematic–smectic transition temperature/°C		<0
Isotropic–nematic transition temperature/°C		114·6
Viscosity (20°C)/mPa s		41·1
Refractive index	n_e	1·650
	n_o	1·502
	Δn	0·148

well as negative dielectric anisotropy (see figure 1). Therefore, the alignment of the TFALC molecules can be controlled by changing the frequency of the applied electric field. Interestingly, the TFALC with a slight amount of salt exhibits a dynamic light scattering (DS) effect when subjected to an electric field whose frequency is near its crossover point (f_0) or slightly higher than f_0 (regime II in figure 1). This behaviour was used for the reversible switching of LCCs.

Montmorillonite is a layered clay mineral composed of aluminosilicates $[(OH)_4Si_8(Al_{3.34}Mg_{0.66})O_{20}{-}Na_{0.66}]$. The dimensions of the unit aluminosilicate layer are only 10 Å in thickness, about 1000 Å in width and length. It has exchangeable cations between the layers, normally sodium cations. In this experiment, the montmorillonite exchanged with 4-cyano(4′-biphenyloxy)undecyl ammonium cation (CBUM, scheme 1) was used to enhance the miscibility between the montmorillonite and TFALC.

Tetrahydrofuran (THF, from Wako Pure Chemical Industries, Ltd.) was dried and distilled over lithium aluminium hydride. Potassium phthalimide, chloroform, anhydrous magnesium sulphate, *n*-hexane, acetone, hydrazine monohydrate, hydrochloric acid, sodium hydroxide (NaOH), tetra-*n*-butylammonium bromide (TBAB), and ethanol (all from Wako Pure Chemical Industries, Ltd.) were used as received. 11-Bromoundecanol, tetrabutylammonium hydrogen

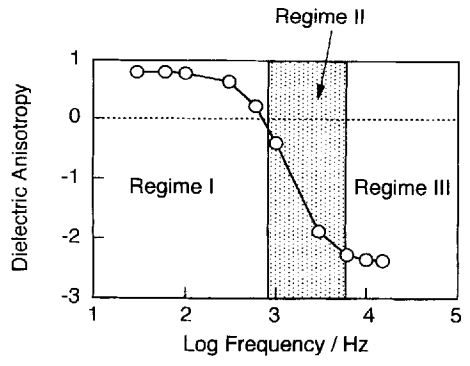

Figure 1. Dielectric anisotropy of the two-frequency-addressing nematic liquid crystal (DF05-XX) as a function of logarithm of frequency.

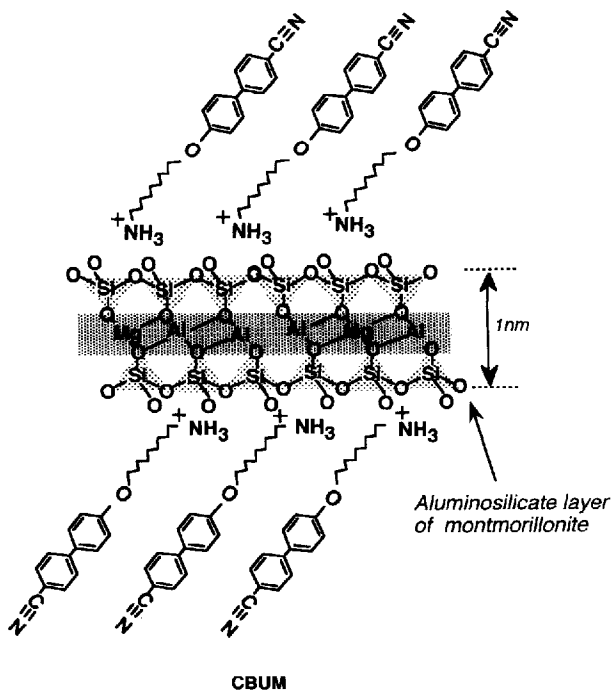

Scheme 1. Schematic representation of montmorillonite intercalated with 4-cyano(4′-biphenyloxy)undecyl ammonium cation.

sulphate, *N*,*N*-dimethylformamide (DMF), carbon tetrabromide, triphenyl phosphine, 4-cyano-4′-hydroxybiphenyl, anhydrous potassium carbonate, *N*,*N*-dimethylacetamide (DMAc) and dimethyl sulphoxide (DMSO) (all from Tokyo Chemical Industry Co., Ltd.) were used as received. Silicagel BW-300 (from Fuji Silysia) was used as received.

2.2. *The preparation of montmorillonite intercalated with 4-(4′-cyanobiphenyl-4-oxy)undecyl ammonium*

The synthetic scheme of 4-(11-aminoundecyloxy)-4′-cyanobiphenyl (**7**) is shown in scheme 2. The detailed procedures are explained as follows.

2.2.1. *Synthesis of* N-*(11-hydroxyundecyl)phthalimide (3)*

To a three-necked flask equipped with nitrogen in–outlets, reflux condenser, and magnetic stirrer, were added 10·0 g (39·8 mmol) of 11-bromoundecanol (**2**), 8·85 g (47·8 mmol) of potassium phthalimide, 0·136 g (0·40 mmol) of tetrabutylammonium hydrogen sulphate, and 20 ml of DMF. The mixture was heated to 80°C with stirring for 7 h. The reaction mixture was poured into 300 ml of water and extracted with 300 ml of chloroform. The organic layer was washed three times with water, and dried over anhydrous magnesium sulphate. The solvent was evaporated on a rotary evaporator to

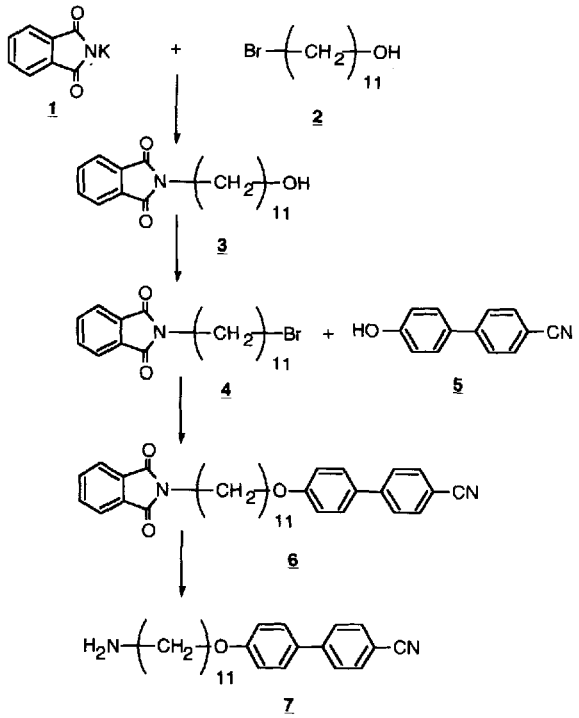

Scheme 2. Synthesis of 4-(11-aminoundecyloxy)-4'-cyanobiphenyl.

yield a solid. It was purified by silica gel column chromatography (solvent: chloroform) followed by the crystallization from *n*-hexane solution to yield white crystals (11·8 g) (yield 93·3 per cent). Melting point 86·6°C.

2.2.2. *Synthesis of* N-*(11-bromoundecyl)phthalimide (4)*

To a three-necked flask equipped with nitrogen in–outlets, reflux condenser, and magnetic stirrer, were added 11·4 g (35·9 mmol) of *N*-(11-hydroxyundecyl)phthalimide (**3**), 12·5 g (37·7 mmol) of carbon tetrabromide, and 20 ml of dry THF. To this mixture, 9·89 g (37·7 mmol) of triphenyl phosphine dissolved in 20 ml of THF was added dropwise. The reaction mixture was stirred at room temperature. After 28 h the reaction mixture was poured into 500 ml of *n*-hexane and the white precipitate was removed. The solvent was evaporated on a rotary evaporator to yield a liquid. It was purified by silica gel column chromatography (solvent: *n*-hexane:chloroform = 1 : 1) followed by the evaporation of bromoform and carbon tetrabromide *in vacuo* to yield a pale yellow liquid (8·15 g) (yield 59·6 per cent). It crystallized by itself. Melting point 48·1°C.

2.2.3. *Synthesis of 4-(11-(*N*-phthalimide)undecyloxy-4'-cyanobiphenyl (6)*

To a three-necked flask equipped with nitrogen in–outlets, reflux condenser, and magnetic stirrer, were added 4·29 g (22·0 mmol) of 4-cyano-4'-hydroxybiphenyl (**5**), 7·60 g (55·0 mmol) of anhydrous potassium carbonate, and acetone–DMSO mixed solvent (60 ml–6 ml). The mixture was heated to the reflux temperature with stirring. After about 3·5 h, 7·74 g (22·0 mmol) of *N*-(11-bromoundecyl)phthalimide (**4**) was added and was stirred for 10 h. The reaction mixture was poured into 400 ml of water and extracted with 300 ml of chloroform. The organic layer was washed three times with 300 ml of water, and dried over anhydrous magnesium sulphate. The solvent was evaporated on a rotary evaporator to produce a pale yellow solid. It was purified by silica gel column chromatography (solvents: *n*-hexane:chloroform = 1 : 1) followed by crystallization from *n*-hexane solution (a slight amount of chloroform was added) to yield white plate-like crystals (6·31 g) (yield 58·0 per cent). Melting point 111·4°C.

2.2.4. *Synthesis of 4-(11-aminoundecyloxy)-4'-cyanobiphenyl (7)*

To a three-necked flask equipped with nitrogen in–outlets, reflux condenser, and magnetic stirrer, were added 5·9 g (12 mmol) of 4-(11-(*N*-phthalimide) undecyloxy-4'-cyanobiphenyl (**6**) and 20 ml of THF. Hydrazine monohydrate (7·26 g, 145 mmol) and 10 ml of ethanol were added and the mixture was stirred for 6 h under reflux. Concentrated hydrochloric acid (55 ml) was added slowly. The reaction mixture was extracted with 300 ml of chloroform and NaOH–water solution (56 g–140 ml). The organic layer was washed three times with water. After it was dried over anhydrous sodium sulphate, the solvent was evaporated on a rotary evaporator to yield a solid. It was purified by silica gel column chromatography (solvents: first time, chloroform only; second time, ethanol:chloroform = 1 : 1) to yield a pale yellow solid (3·82 g) (yield 86·4 per cent). Melting point 82·5°C, clearing temperature 117·7°C.

2.2.5. *Intercalation*

Sodium montmorillonite (2·00 g, cation exchange capacity: 2·38 meq) was dispersed in 70 ml of hot water (about 50°C). 4-(11-Aminoundecyloxy)-4'-cyanobiphenyl (**7**) (0·955 g, 2·62 mmol) and concentrated hydrochloric acid (0·28 g) were dissolved into a hot ethanol and water mixture (40 ml : 10 ml). It was poured into the hot montmorillonite–water solution with vigorous stirring to yield a white precipitate. After 3 h the precipitate was collected on a glass filter, washed with ethanol and twice with hot water, and freeze-dried to yield a montmorillonite intercalated with 4-(4'-cyanobiphenyl-4-oxy)undecyl ammonium (CBUM, see scheme 1). We measured the interlayer distance between the layers of the clay intercalated with CBUM by X-ray diffraction, and its inorganic content by measuring the weights before and after burning the organic

parts of the clay. The interlayer distance of the sodium montmorillonite was 12 Å while that of the CBUM was 20·4 Å. The measured inorganic content of the CBUM was 70·5 wt % which is almost equal to the expected value of 69·1 wt %. (The expected value was calculated from the ion exchange capacity (119 meq/100 g of sodium montmorillonite) and molecular weight of cyanobiphenyl ammonium). These results clearly indicate the quantitative intercalation of cyanobiphenyloxy alkyl ammonium in the clay.

2.3. *The preparation of LCCs consisting of TFALC and CBUM*

The composites based on TFALC and CBUM were prepared as follows. CBUM (0·0181 g) was dispersed into DMAc and mixed with 1·0 g of TFALC and 0·200 g of TBAB/DMAc solution (TBAB/DMAc = $1·02 \times 10^{-4}$ g/g). DMAc was evaporated *in vacuo* at 50°C for 10 h and the obtained composite was mechanically stirred. It was dried *in vacuo* at 50°C for 10 h to yield a white pasty composite (LCC-1·25, the content of the inorganic part, 1·25 wt %).

Six other composites with different inorganic contents (LCC-0·20, LCC-0·50, LCC-1·00, LCC-1·50, LCC-1·75, and LCC-2·00; the contents of the inorganic parts were 0·2 wt %, 0·5 wt %, 1·00 wt %, 1·50 wt %, 1·75 wt % and 2·00 wt %, respectively) were prepared by the same method.

2.4. *Techniques*

A Perkin–Elmer DSC-7 differential scanning calorimeter (DSC) was used to determine thermal transitions of synthesized compounds. Heating rates were 10°C min^{-1} in all cases. An Olympus Model BHSP optical polarizing microscope (magnification, 500 ×) equipped with a Mettler FP-82HT hot stage and Mettler FP-90 central processor was used to observe thermal transitions and to analyse anisotropic textures. X-ray powder diffraction studies of the clay minerals were obtained by using a Rigaku RAD-B diffractometer with CuKα radiation to measure the interlayer distances of the clay minerals.

Figure 2 shows a schematic representation of the system set-up for the optical measurement of the LCC cells. The substrates of the cells were 1·1 mm thick glass plates coated with a thin transparent conductive In/SnO_2 (ITO) film to allow the application of an electric field across the LCC. The separation of the substrates was achieved by sandwiching the two plates with polymer bead spacers (diameter: 12 μm), thus defining the thickness of the LCC. The electro-optic effect was measured by using the BHSP microscope equipped with a photomultiplier to monitor the optical change in the cell accompanying the application of the electric field across

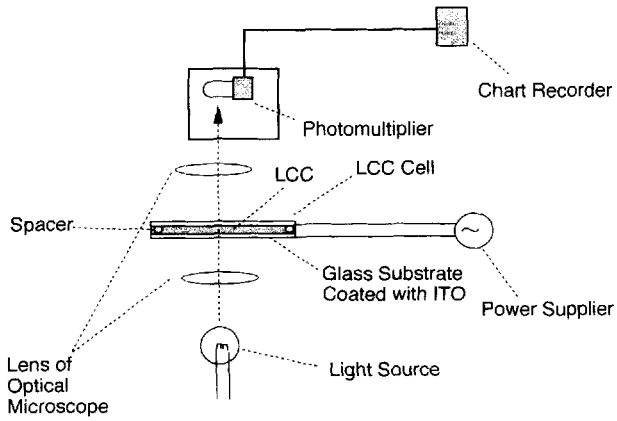

Figure 2. Schematic representation of the system set-up for the optical measurements of the LCC cells.

the samples (in this case, the microscope was used without polarizers). These were recorded on a chart recorder. The power supply (100 V–60 Hz, sin wave) with voltage adjusted using a Slidac was used for applying the low frequency electric field (60 Hz) to the cell. A power amplifier Model S-4750 manufactured by the NF Electronic Instruments co. was used for applying the high frequency electric field (1–1·5 kHz). The light transmittance of the cell was calculated according to equation (1). All measurements were carried out at room temperature.

$$\text{Light transmittance (per cent)} = \frac{100 \times (\text{photomultiplier value of sample cell})}{(\text{photomultiplier value of blank cell sealed with water})} \quad (1)$$

3. Results and discussion

3.1. *Characterization of the obtained LCC*

The clay with sodium cations is extremely hydrophilic and easily dispersed in water, but not in liquid crystals which are normally hydrophobic. We tried to prepare the composites with sodium montmorillonite. However, we found that the relatively large (about few hundreds μm) precipitation of the clay particles occurred in the liquid crystals.

In the case of the clay intercalated with 4-(4′-cyanobiphenyl-4-oxy)undecyl ammonium, the particles of the clay dispersed in the liquid crystal far better than the case of the sodium clay. Figure 3 shows typical polarized micrographs of the obtained LCC-1·25 in the (*a*) isotropic state and (*b*) nematic state. In the isotropic state, only the particles of CBUM were observed as white spots which were dispersed uniformly in the LCC. Their sizes were roughly estimated to be several μm or less. They are considered to be the aggregates of unit layers of CBUM. On the other hand, the very fine

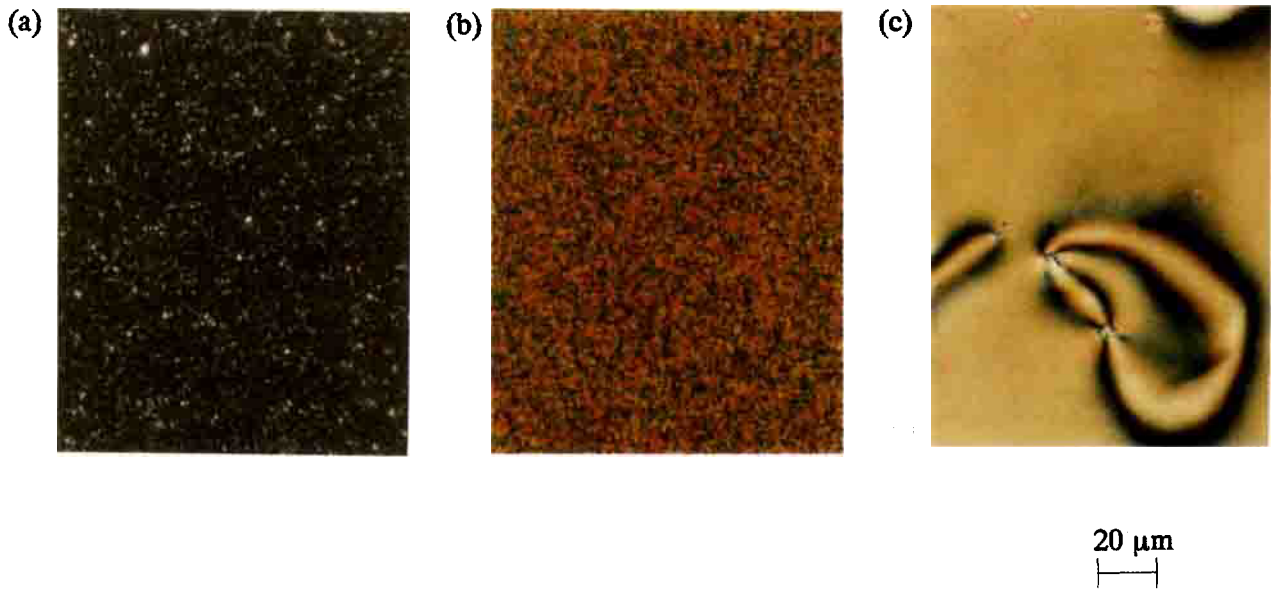

Figure 3. Optical polarized micrographs of LCC and TFALC (crossed nicols, the thickness of the sample is 12 μm): (*a*) isotropic state of the LCC, (*b*) nematic state of the LCC, and (*c*) nematic state of the TFALC.

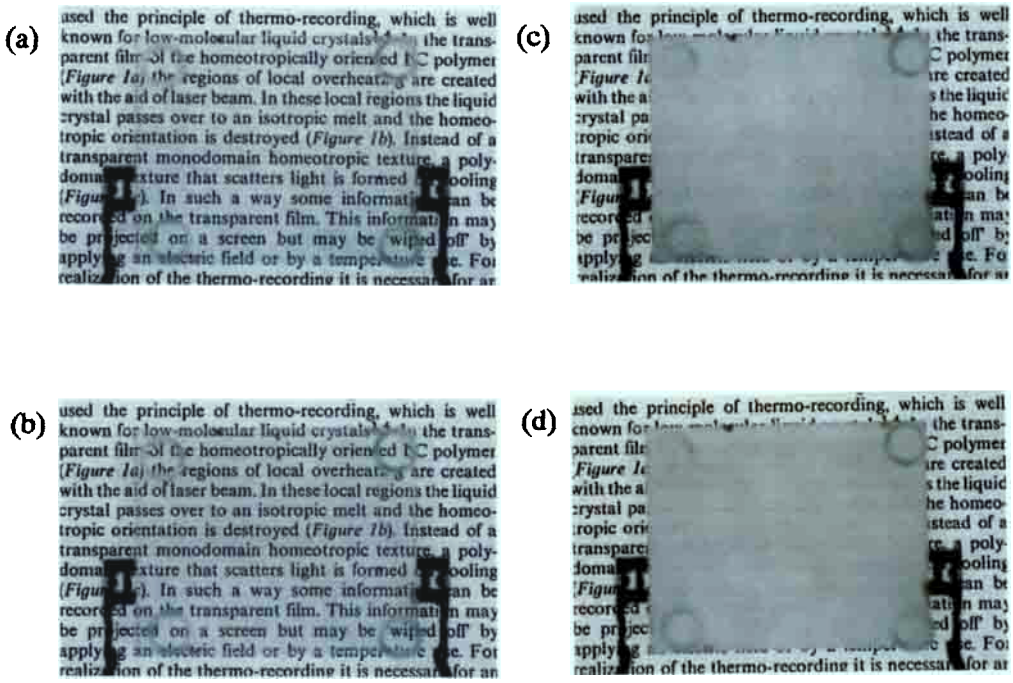

Figure 5. Photographs of the LCC-1·25 cell (cell gap: 12 μm) at various states: (*a*) on-state I (50 V–60 Hz), (*b*) memory state I (60 Hz OFF), (*c*) on-state II (100 V–1·5 kHz), (*d*) memory state II (1·5 kHz OFF).

texture of the LCC was observed in the nematic state. The texture is composed of very small domains of TFALC (multi-domain structure). Since pure TFALC does not exhibit such a fine texture (see figure 3 (*c*)), we conclude that CBUM induced the multi-domain structure in the LCC as discussed previously [6].

3.2. *Electro-optical properties of the LCC*

The LCC-1·25 cell displayed a reversible and bistable electro-optical effect based on light scattering which could be controlled by changing the frequency of the electric field. Figure 4 shows a typical change in the light transmittance of the LCC-1·25 cell (bold line) as well as

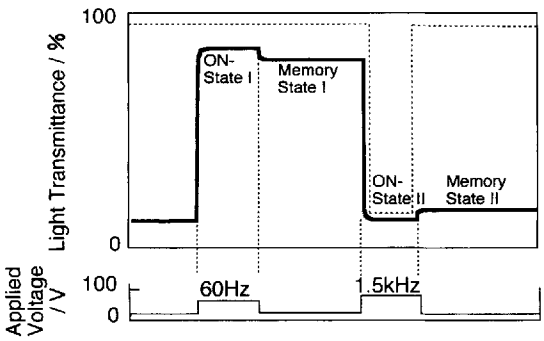

Figure 4. The change in the transmittance of the LCC-1·25 cell (cell gap: 12 μm) by two frequency driving (driving sequence: 60 Hz–50 V ON, 60 Hz OFF, 1·5 Hz–100 V ON, 1·5 kHz OFF).

of a TFALC cell (broken line) when the cells were subjected to electric fields. Figure 5 presents the photographs of the LCC-1·25 cell at various states. When a low frequency electric field (60 Hz–50 V, regime I in figure 1) was applied to the cell, it became transparent within 50 ms (on-state I in figure 4, figure 5(*a*)). Even after the electric field was switched off, although a small decrease in the transparency was observed, the transparent state was maintained (memory state I in figure 4, figure 5(*b*)). When a high frequency electric field (1·5 kHz–100 V, regime II in figure 1) was applied to the cell, the memory state I was cancelled to return to the light scattering state (on-state II in figure 4 and figure 5(*c*)) within 50 ms. Again, although a small increase in the transparency occurred, the light scattering state was maintained without the electric field (memory state II in figure 4, figure 5(*d*)). The alternative application of both the high frequency and the low frequency electric fields was repeated 100 times and almost no change in the light transmittances of the cell in the all states was found. On the other hand, as seen in figure 4, the TFALC cell did not exhibit such a memory effect.

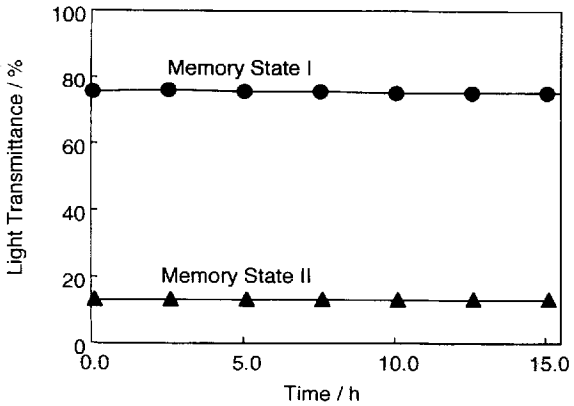

Figure 6. The stabilities of the memory state I and memory state II of the LCC-1·25 cell.

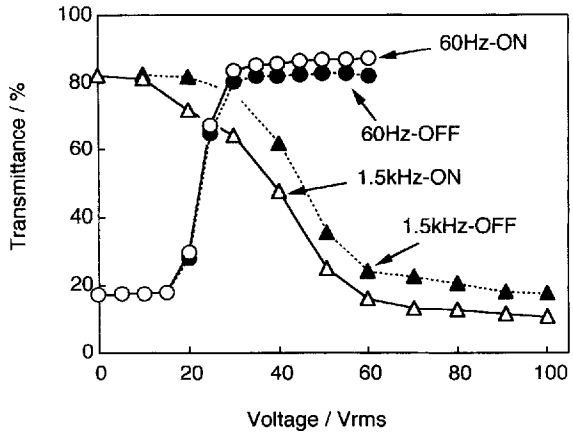

Figure 7. Transmission properties of the LCC cells in the on-state I (60 Hz ON), memory state I (60 Hz OFF), on-state II (1·5 kHz ON), memory state II (1·5 kHz OFF) as a function of the applied voltage.

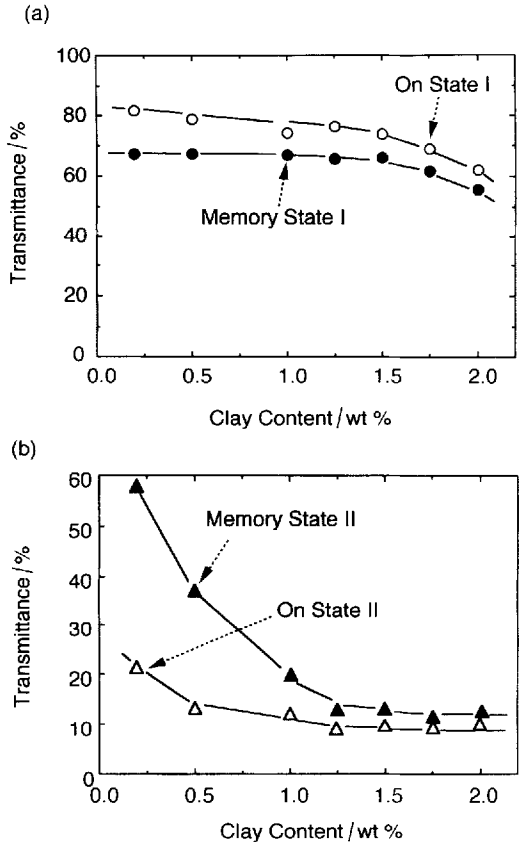

Figure 8. (*a*) Saturated transmittance of the LCC cells in the on-state I (60 Hz ON) and memory state I (60 Hz OFF) as a function of the CBUM content; (*b*) saturated transmittance of the LCC cells in the on-state II (1 kHz ON), memory state II (1 kHz OFF) as a function of the CBUM content (based on a inorganic part).

The light transmittances of the memory states I and II of LCC-1·25 did not change after 15 h as indicated in figure 6. Although the LCC is based on a nematic liquid crystal, it exhibited an unusual stability of the memory states.

Figure 7 shows the transmittance of the LCC-1·25 cell as a function of applied voltage. Open and closed circles indicate the transmittance of the cell in the on-state I and memory state I, respectively. (A low frequency electric field (60 Hz) was applied to the cell which had initially been in the memory state II created by applying 1·5 kHz–100 V). On the other hand, open and closed triangles indicate the transmittance of the cell in the on-state II and memory state II. (A high frequency electric field (1·5 kHz) was applied to the cell in the memory state I created by applying 60 Hz–50 V.) The transmittance of the cell in the on-state I and the memory state I start to increase around 20 V_{rms} and saturate about 40 V_{rms}. On the other hand, the transmittance of the cell in the on-state II and memory state II start to decrease around 20 V_{rms} and saturate over 60 V_{rms}. Any level of transmittance in the memory state can be achieved by adjusting the applied voltage.

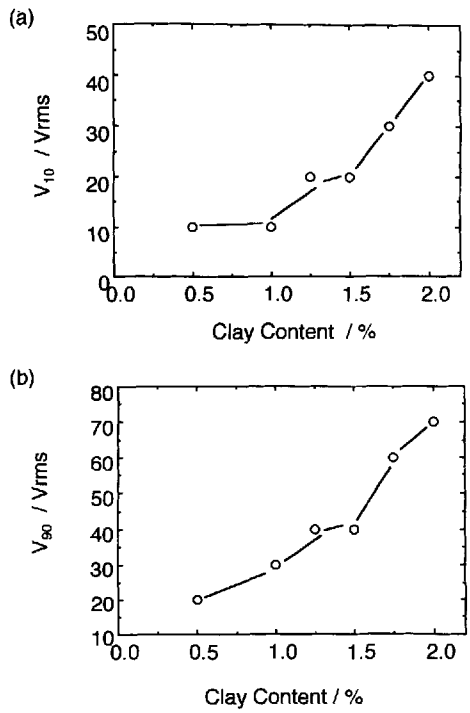

Figure 9. (*a*) Plots of V_{10} (the voltage at which the light transmittance becomes the 10 per cent of the maximum value) and (*b*) V_{90} (the voltage at which the light transmittance becomes the 90 per cent of the maximum value) of the LCC cells in on-state I (60 Hz) as a function of the CBUM content (based on the inorganic part). Clay content in wt%.

3.3. *Dependence of electro-optical properties of the LCC on the clay content*

In figures 8 (*a*) and (*b*), the transmittance of the LCC cells was plotted as a function of the clay content. Figure 8 (*a*) indicates the saturated maximum transmittance of the cells in the transparent on-state I (white circle) and memory state I (black circle), while figure 8 (*b*) indicates the saturated minimum transmittance of the cell in the opaque on-state II and memory state II. As seen from figure 8 (*a*), the maximum transmittance of the LCC cells in both the transparent states tend to increase with decreasing the clay content. On the other hand, with decreasing the clay content, the minimum transmittance of the LCC cells in the on-state II increases gradually, while that in the memory state II increases abruptly from around 1·0 wt %, thus decreasing the memory effect. These results indicate the most effective clay content to obtain the highest contrast between memory state I and memory state II is around 1·25 wt %.

Figures 9 (*a*) and (*b*) show the plots of V_{10} (the voltage at which the light transmittance becomes 10 per cent of the maximum value) and V_{90} (the voltage at which the light transmittance becomes 90 per cent of the maximum value) of the LCC cells in the on-state I against the clay content. Both V_{10} and V_{90} increase with increasing clay content. The same trend was observed for the plots of

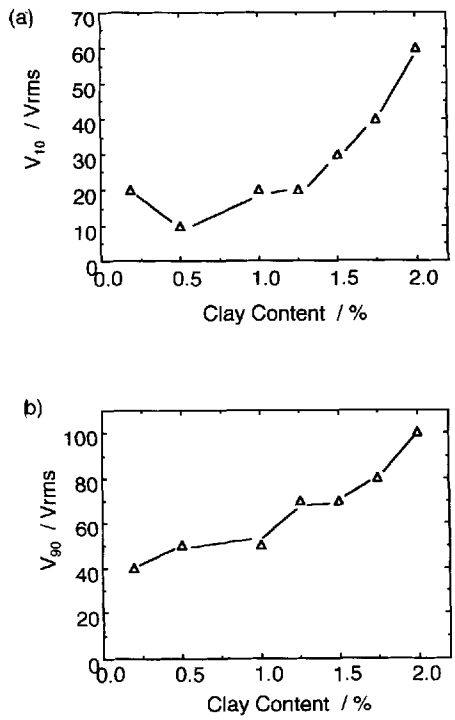

Figure 10. (*a*) Plots of V_{10} and (*b*) V_{90} of the LCC cells in on-state II (1 kHz) as a function of the CBUM content (based on the inorganic part). Clay content in wt%.

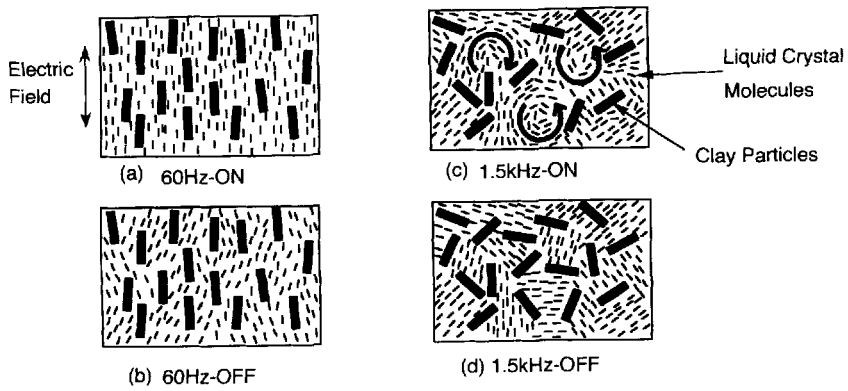

Figure 11. The schematic representation of the LCC structure at various states: (*a*) on-state I, (*b*) memory state I, (*c*) on-state II, (*d*) memory state II.

V_{10} and V_{90} of the LCC cells in the on-state II as indicated in figures 10(*a*) and (*b*).

3.4. *Possible mechanism of the memory effect*

Let us consider the possible mechanism of the memory effect in the LCC. Figure 11 presents a schematic explanation of the memory mechanism. When a low frequency electric field in regime I is applied to the cell, not only the TFALC but also CBUM plates align parallel to the electric field as demonstrated previously [6] (see figure 11(*a*)), and the cell becomes transparent. Even after the electric field is switched off, the plates maintain their orientation due to their bulkiness. As a result, the TFALC molecules maintain their homeotropic alignment to produce the memory state I (see figure 11(*b*)).

On the other hand, when a high frequency electric field is applied, a turbulent motion of TFALC molecules as well as CBUM plates occurs in the cell to exhibit a strong light scattering (see figure 11(*c*)). After the electric field is switched off, the alignments of the plates become random to produce a multidomain structure of the liquid crystal in the cell (see figure 11(*d*)). In the multidomain, the nematic director of each domain is considered to orient randomly in space. The fluctuation of the refractive indexes is maintained in the LCC and scatters light. Therefore, the light scattering state is maintained as memory state II. However, if there is not a sufficient clay content to maintain the multidomain structure, the memory effect becomes weak as discussed above. The increase in the driving voltage with increasing clay content should be attributed to the fact that the change in alignment of the clay particles as well as the TFALC molecules should take place to change to the state as discussed above. Therefore, the LCC requires a stronger electric field than the TFALC alone. Also the interaction between the TFALC and clay particles might increase the threshold voltage of the TFALC in the LCC.

4. Conclusions

By mixing a two-frequency-addressing liquid crystal and organophilic clay mineral, we have created novel liquid crystalline composites in which the plates of the clay mineral were homogeneously dispersed in micrometer level. The composite cells exhibited a bistable and reversible light scattering effect which could be controlled by changing the frequency of the applied electric field. This new material would be a potential candidate for advanced applications such as a light controlling glass, a high information display device which does not require active addressing, an erasable optical storage device, and so on. Also, the results shown in this paper open a new opportunity to synthesize a variety of liquid crystalline composites and extend the function of liquid crystals.

References

[1] Heilmeier, G. H., and Goldmacher, J. E., 1968, *Appl. Phys. Lett.*, **13**, 132.
[2] Kajiyama, T., Kikuchi, H., Miyamoto, A., Moritomi, S., and Hwang, J. C., 1989, *Chem. Lett.*, **1989**, 817.
[3] Yamaguchi, R., and Sato, S., 1993, *Liq. Cryst.*, **14**, 929.
[4] Cheng, J., 1982, *J. appl. Phys.*, **53**, 5584.
[5] Barberi, R., 1992, *Appl. Phys. Lett.*, **60**, 1085.
[6] Kawasumi, M., Usuki, A., Okada, A., and Kurauchi, T., 1996, *Mol. Cryst. liq. Cryst.*, **281**, 91.